ELSEVIER

Journal of Magnetism and Magnetic Materials 161 (1996) 337–356

Journal of magnetism and magnetic materials

Numerical simulations of quasistatic remagnetization processes in fine magnetic particle systems

D.V. Berkov *

Institut für Physikalische Hochtechnologie, Helmholtzweg 4, D-07734, Jena, Germany

Received 18 August 1995; revised 29 January 1996

Abstract

Various numerical methods used for simulation of quasistatic remagnetization processes in interacting systems of fine single-domain magnetic particles are analyzed. Among them methods based on the sequential alignment of magnetic moments along the effective field are found to be the fastest, especially in the most interesting case of a small single particle anisotropy when cooperative remagnetization modes play a dominant role. Further it is shown, that the random field approximation (RFA) which is often used to take the interparticle interaction effects into account is valid for large particle anisotropies only. The distribution density of the interaction field is found to transform from the Lorentzian to the Gaussian form with the increasing particle volume fraction. Finally hysteresis loops for a wide range of single-particle anisotropy values and particle concentration are calculated and the crossover from the single particle to the collective behavior with decreasing single particle anisotropy is investigated.

Keywords: Fine magnetic particles; Numerical simulations; Remagnetization processes

1. Introduction

Numerical simulations of quasistatic remagnetization processes in systems of fine magnetic particles are widely used now. They are a powerful tool in applied physics, where simulations of magnetic recording processes in particulate media [1–4] and of ferrofluids [5] are of a great practical interest. By studying fundamental problems connected with the spin-glass-like behavior of magnetic dipole glasses [6–8] and strongly interacting fine magnetic particle systems [1,9] these methods are also very important and in many cases even unique because analytical treatments are mostly unavailable for such systems.

Despite quite a long history of numerical methods created to simulate a quasistatical behavior of interacting fine magnetic particle systems some basic questions are not yet settled. From the methodological point of view we still lack a detailed comparative analysis of the performance of different methods for various system parameters. It would be also highly desirable to find out, for which system parameters (first of all for which particle anisotropies and volume concentrations of the ferromagnetic phase) a so called random field approximation (RFA) provides adequate results and hence can be used as a much faster alternative to 'real' simulations. A most important physical problem connected with the quasistatical remagnetization processes at temperatures much

* Permanent address: Institute of Chemical Physics, 142432 Chernogolovka, Russian Federation

PII S0304-8853(96)00070-4

lower than characteristic energy barriers in the system concerns the crossover from the single-particle-like behavior for large values of the single-particle anisotropy to collective remagnetization modes when the anisotropy decreases and interparticle interactions start to play a dominant role.

This paper is organized as follows. In Section 1 we analyze the behavior of three main groups of numerical methods used for simulations of fine particle systems: (i) standard conjugate gradient method for the minimization of functions of many variables, (ii) methods which use the Landau–Lifshitz-like 'equations of motion' for a magnetic moment in an effective field and (iii) methods based on the alignment of magnetic moments along the total effective field at the given point. We show that properly organized alignment methods are superior to other methods (especially for low particle anisotropies) and discuss principal problems connected with conjugate gradient methods and some possible improvements of methods based on the Landau–Lifshitz relaxation.

In Section 2 the random field approximation is discussed in detail. We study the form of the interaction field distribution density for various particle volume fractions and demonstrate that this distribution evolves from the Lorentzian to the Gaussian one when the particle concentration increases. Comparing results of 'real' simulations and RFA calculations we find out the parameter region on the anisotropy–concentration plane where the RFA approximation is valid.

Section 3 contains physical results concerning primary the dependence of the coercivity and remanence of the system studied on the single-particle anisotropy strength and the particle volume concentration. The transition from the single-particle to the collective behavior when the particle anisotropy decreases is also discussed. In conclusion we summarize our results and open problems.

2. Comparison of numerical methods for simulations of remagnetization processes

In disordered systems with the anisotropic long range interparticle interaction there exist many metastable states. This leads to the well known difficulties by describing the thermodynamics of such systems [6,10] because for the finite temperature all possible transitions between a huge variety of these metastable states should be properly accounted for. The task to simulate quasistatic remagnetization processes for low temperatures when all energy barriers are much higher then the thermal activation energy is in this sense much simpler: at these low temperatures we can neglect thermal activation processes and consider only magnetization changes due to the evolution of the energy 'landscape' of the system in the varying external field.

Usually one starts from the large (saturating) external field where only one (true) equilibrium state exists. When the external field decreases adiabatically in magnitude and then changes its direction the equilibrium state which emerges from this initial true equilibrium becomes metastable, because other states with lower energies appear. However, they are separated from the state which results from the continuous evolution of the initial state by energy barriers which are assumed to be infinitely high in the zero temperature limit. This means that the system remains in this metastable state until it disappears by a certain field value and then jumps into one of the low-lying (may be also only metastable) states.

The remagnetization scenario described above means that by simulations of such processes we are always interested in that energy minimum which is the closest one to the (meta)stable state of the system obtained for the previous field value. This means, in turn, that we are not concerned with the problem to find the global energy minimum but merely with the task to achieve the neighbouring local one when starting from the given system state (this assumption is implicitly used practically in all papers devoted to such simulations).

Realizing this greatly simplifying circumstance, one can adopt one of the following strategies:

(i) Apply some standard numerical method for many-variable function minimization to find the local minimum of the system energy as a function of particle magnetic moment orientations starting from the equilibrium state achieved in the previous magnetic field.

(ii) Solve the system of equations of motion for magnetic moments in the effective field (i.e., in the Landau–Lifshitz–Gilbert form). The dissipative term

present in such equations drives the system towards the equilibrium so that for sufficiently long integration time a system state arbitrary close to the equilibrium can be achieved.

(iii) Organize an iteration procedure based on the fact that in the equilibrium state each magnetic moment is aligned parallel to the corresponding effective field. A simple alignment of each moment along this field for each iteration may not work, as we shall see below, but it is always possible to construct a closely related algorithm which surely converges.

2.1. Evaluation of the system energy

Before starting comparative analysis of three method groups listed above, we shall briefly discuss the problem of the evaluation of the system energy E_{tot}. This energy is explicitly required for the implementation of methods belonging to the first and second groups and may also be helpful for the organization of the surely converging alignment methods.

For a system of single-domain particles with no exchange interaction between particles the total system energy is a sum of three contributions: energy in an external field E_{ext}, anisotropy energy E_{an} and the interparticle interaction energy E_{int}:

$$E_{\text{tot}} = -\sum_i \boldsymbol{\mu}_i \boldsymbol{H}_i^{\text{ext}} - \sum_i \frac{\beta_i}{2} M_s^2 V_{0i} (\boldsymbol{m}_i \boldsymbol{n}_i)^2 - \frac{1}{2} \sum_i \boldsymbol{\mu}_i \boldsymbol{H}_i^{\text{int}}. \quad (1)$$

Here the first term represents the energy of magnetic moments $\boldsymbol{\mu}_i$ in the external field (which may be non-homogeneous) $\boldsymbol{H}_i^{\text{ext}} \equiv \boldsymbol{H}^{\text{ext}}(\boldsymbol{r}_i)$, $\boldsymbol{r}_i$ being the radius-vector of ith particle. The form of the second term describing the anisotropy energy corresponds to the uniaxial single-particle anisotropy, whereby unit vectors $\boldsymbol{n}_i$ and $\boldsymbol{m}_i$ give the directions of the anisotropy axis and magnetic moment correspondingly, M_s denotes the material magnetization and V_{0i} the particle volume. Reduced anisotropy constants β_i are positive for the 'easy-axis'-case. Often another expression for the anisotropy energy is used: $E_{\text{an}} = -KV_0(\boldsymbol{mn})^2$. It is easy to verify that the relation between the anisotropy constant K used in this notation and β in Eq. (1) is $\beta = 2K/M_s^2$.

In the third term representing the interparticle dipole–dipole interaction energy the interaction (dipole) field which is created at the location of the ith particle by all other particles of the system

$$\boldsymbol{H}_i^{\text{int}} = \sum_{j \neq i} \boldsymbol{H}_{ij}^{\text{dip}} = \sum_{j \neq i} \frac{3\boldsymbol{e}_{ij}(\boldsymbol{e}_{ij}\boldsymbol{\mu}_j) - \boldsymbol{\mu}_j}{r_{ij}^3} \quad (2)$$

is used. Here $\boldsymbol{r}_{ij} = \boldsymbol{r}_i - \boldsymbol{r}_j$ and a unit vector $\boldsymbol{e}_{ij} = \boldsymbol{r}_{ij}/r_{ij}$ is introduced.

The first and second energy terms are local in the sense that the evaluation of the corresponding effective field contributions for the given particle requires only local information about the moment orientation and the anisotropy axis direction of this particle. This means that the evaluation of these energies requires only $\sim N$ operations for a system of N particles. But the interaction field term for the given particle includes contributions from all other particles and hence the evaluation of the corresponding energy is an $\sim N^2$-process, i.e., a computational time grows very rapidly with the particle number. This means that if the interaction field is calculated using the straightforward summation as indicated in Eq. (2) then the maximal number of particles in the simulated system may not exceed $\sim 2 \times 10^4$ even when modern supercomputers are used [11].

The problem is exactly the same as in classical micromagnetics [12]. The latter deals with the determination of the equilibrium magnetization structures of large ferromagnetic bodies and due to the N^2-dependence the evaluation of the interaction energy (also called demagnetizing or stray field energy) is always the most time-consuming part of any micromagnetical algorithm. If a rectangular discretization grid can be applied, one can use fast Fourier transform methods for the evaluation of Eq. (2) because for the translationally invariant grid this sum can be calculated as a discrete convolution [13,14]. In this case the number of finite elements used for a discretization of a problem can achieve $\sim 10^5$ [13,14].

But in all calculations of magnetization structures where a nonuniform discretization was necessary (usually due to the complicate sample shape), the number of corresponding finite elements did not exceed $\sim (2\text{–}5) \times 10^2$ [15–18]. And in fine particle simulations the problem is even more serious, because to obtain physically meaningful results one

should perform (for one set of system parameters) calculations for various particle configurations because the averaging over various realizations of the spatial disorder is necessary [6,10].

Fortunately, if we are interested in simulations of magnetization processes in a homogeneous external field and in globally homogeneous particle systems (whereby local fluctuations due to a spatial disorder are of course present) it is possible to divide a space around the given particle into the near and far regions using some restriction radius R_r [19–21]. A contribution to the interaction field on the given particle from all particles which are inside the near region ($r_{ij} < R_r$) is calculated explicitly using Eq. (2) where the summation is performed only over those neighbors for which $r_{ij} < R_r$. The system outside the sphere with the radius R_r is considered as a homogeneous medium, which leads to the well known Lorentz field contribution from this part of the system. Hence the interaction field on the given particle can be calculated as

$$\boldsymbol{H}_i^{\text{int}} = \sum_{j \neq i} \boldsymbol{H}_{ij}^{\text{dip}} = \sum_{r_{ij} < R_r} \frac{3\boldsymbol{e}_{ij}(\boldsymbol{e}_{ij}\boldsymbol{\mu}_j) - \boldsymbol{\mu}_j}{r_{ij}^3} + \frac{4\pi}{3}\langle \boldsymbol{M} \rangle - \hat{D}\langle \boldsymbol{M} \rangle, \tag{3}$$

where $\langle \boldsymbol{M} \rangle$ denotes the average system magnetization and $\hat{D}$ is the demagnetization coefficient tensor depending on the sample form only. A suitable R_r-value can be found by increasing this parameter and choosing a value after which physical characteristics of interest (i.e. system magnetization) do not change within the given accuracy. For most kinds of measurements it is sufficient to take $R_r = 3\bar{r}$, where $\bar{r}$ denotes an average interparticle distance [19,20].

We point out here, that for simulations of magnetic recording processes the approximation of Eq. (3) can *not* be used, because a long-range bit structure always present by such simulations does not allow to consider a system as homogeneously magnetized even on a large scale.

In this paper we restrict ourselves to a consideration of systems of identical spherical particles with the radius a and material magnetization M_s. In this case all magnetic moments have the same absolute value and can be written as $\boldsymbol{\mu}_i = V_{0i} M_s \boldsymbol{m}_i = (4\pi/3) a^3 M_s \boldsymbol{m}_i$ where V_{0i} is the volume of the ith particle and $\boldsymbol{m}_i$ is a unit vector pointing in the magnetic moment direction. It is convenient to introduce a reduced field $\boldsymbol{h} = \boldsymbol{H}/M_s$ and a reduced energy $\tilde{E} = E/V_{0i}M_s^2$ and to measure all distances in units of a (we do not introduce special notation for this reduced distances) so that the final energy expression takes the form

$$\tilde{E}_{\text{tot}} = -\sum_i \boldsymbol{m}_i \boldsymbol{h}_i^{\text{ext}} - \sum_i \frac{\beta_i}{2}(\boldsymbol{m}_i \boldsymbol{n}_i)^2 - \frac{1}{2}\sum_i \boldsymbol{m}_i \boldsymbol{h}_i^{\text{dip}}, \tag{4}$$

with the dipole field

$$\boldsymbol{h}_i^{\text{int}} = \frac{4\pi}{3} \sum_{r_{ij} < R_r} \frac{3\boldsymbol{e}_{ij}(\boldsymbol{e}_{ij}\boldsymbol{m}_j) - \boldsymbol{m}_j}{r_{ij}^3} + \frac{4\pi}{3}\eta\langle \boldsymbol{m} \rangle, \tag{5}$$

where η denotes a particle volume concentration.

2.2. Conjugate gradient minimization methods

Standard numerical methods which can be used to minimize the system energy (Eq. (4)) are the steepest descent method, conjugate gradients and various quasi-Newton (also called variable metric) methods [22,23]. The steepest descent method is know for its slow convergence due to its feature to perform many small iteration steps when going down the long and narrow 'valley' even for functions with a relatively simple contour surfaces. Each iteration of various quasi-Newton methods require $\sim N^2$ operations to update sequential approximations for the inverse Hessian $L \times L$ matrix H of the system (L is a number of independent variables). Another drawback of these methods is an additional memory required to store H. This means that for a system of $N = 10^3$ particles storage for $L^2 = (2N)^2 = 4 \times 10^6$ matrix elements is needed, which is also a serious disadvantage. On the other hand, quasi-Newton methods do not offer any specific advantages over conjugate gradients.

The reasons given above mean that conjugate gradient methods are the only reasonable candidates among standard numerical methods used for function minimization [22,23]. Indeed, they are used by several groups involved in classical micromagnetical [24] and fine particle [25] simulations. We have

studied the performance of these methods when applied to the hysteresis loop simulations of fine magnetic particle systems.

First of all we note that to implement conjugate gradients we should transfer from the Cartesian moment coordinates to the spherical ones despite that formulas for the effective field and energy evaluation are in spherical coordinates more complicate. The reason is that during the remagnetization process the magnitude of the magnetic moment should remain constant ($|\mu| = V_0 M_s$) and hence its cartesian coordinates are subject to the restriction $\mu_x^2 + \mu_y^2 + \mu_z^2 =$ constant or (using a unit vector $\boldsymbol{m}$ introduced above) $m_x^2 + m_y^2 + m_z^2 = 1$. This means that Cartesian moment components are dependent variables which does not allow to use them by the implementation of conjugate gradients because the construction of a set of conjugate directions obviously fails when dependent variables are used.

Transition to spherical coordinates (m_x, m_y, $m_z \rightarrow \theta_m$, ϕ_m) leads however to another well known technical problem [24,26]: if a particle moment is sufficiently close to the polar axis ($\theta_m \approx 0$ or $\theta_m \approx \pi$) then its small movements can lead to arbitrary changes of ϕ_m. If not properly avoided, this instabilities result in the best case in a very slow convergence of the method and often even in a failure to build up a corresponding set of conjugate directions so that the method stuck at some intermediate magnetization state.

The solution of this problem in micromagnetics is known [24]: one chooses for each moment a separate spherical coordinate system, the polar axis of which is sufficiently far from the current moment direction (actually it is usually enough to choose between two different spherical coordinate systems with the polar axis along, say, z- and x-axis of Cartesian coordinates). This idea works quite well in classical micromagnetic problems, where one is usually able to start from the state which is not very different from the final solution so that no large movements of magnetic moments are expected. The situation in fine particle simulations is more difficult: after the field has been changed, a particle can 'switch' so that the direction of its moment can change by an amount $\sim \pi$ whereby the trajectory of such a moment movement on the unit sphere may be arbitrary complicated.

The latter circumstances forces to implement the conjugate gradient algorithm for our problem in the following way. For each field we start from the equilibrium magnetization state obtained for the previous field value (for the first field value we begin with the saturated state). We check for each moment whether its direction is sufficiently close to the z-axis chosen as a field direction. If the angle ψ between the moment and this axis is less than some prescribed value $\psi \leq \psi_{cr}$, we choose for this moment a spherical coordinate system of the second kind (i.e., with the polar axis along the x-axis of our Cartesian coordinates). In the opposite case $\psi > \psi_{cr}$ we assign to this moment a spherical coordinate system of the first kind.

When performing energy minimization for the given field value we check by each function evaluation for each moment whether it has approached a polar axis of its spherical coordinates. If for any moment $\theta \leq \theta_{cr}$ (where θ_{cr} is another critical angle) then we change the spherical coordinate system for this moment and restart conjugate gradients from the current magnetization state, because due to the coordinate system change all information collected about the conjugate direction set is lost.

Obviously the performance of a method constructed this way depends on the critical angle values ψ_{cr} and θ_{cr} used to choose between two coordinate systems and to decide whether the algorithm should be restarted. The only a priori ideas concerning the choice of concrete values for these angles are the following:

ψ_{cr} should be ~ 1, because in the most interesting region where remagnetization of the most particles takes place, the external field has the same order of magnitude as the anisotrophy or interaction field so that neither space direction should be preferred in advance

θ_{cr} should not be too small, because very small θ-values lead to the instabilities described above. Too large θ_{cr}-values would cause the algorithm to restart too often (because for large θ_{cr} it is more likely that for some particle we encounter $\theta < \theta_{cr}$), which obviously leads to the loss of efficiency.

We investigated this question 'experimentally' performing simulations for various system parameters and found that optimal values for these angles are $\psi_{cr} \approx \pi/4$ and $\psi_{cr} \approx \pi/40$, whereby the mini-

mum of the computational time as a function of ψ_{cr} and θ_{cr} achieved around the values given above is quite flat.

As a termination criterion we have used a smallness of a rotational force moment acting on each magnetic moment: we stop our minimization process if for all moments $\|[\boldsymbol{m}_i \times \boldsymbol{h}_i^{\text{eff}}]\| < \epsilon$ where ϵ is some constant. We found that $\epsilon = 10^{-3}$ was small enough in the sense no further changes in the equilibrium magnetization state were observed if smaller ϵ were used. This criterion provides information about the state of each magnetic moment and hence is more sensitive than another often used criterion when the minimization process is terminated if the total system energy change after one iteration is sufficiently small.

Computational times for various anisotropy values β are presented in Fig. 4, where data for conjugate gradients are shown with open circles. We shall discuss these dependencies later after a description of two other method groups.

2.3. *'Equations-of-motion' methods*

These methods are very popular both by treating classical micromagnetic problems [14,26–28] and by simulating fine particle systems [21,29] due to their physical transparency, guaranteed convergence and a large variety of mathematical methods invented to solve systems of ordinary differential equations.

The basic idea is to build up a relaxation procedure using equations of motion for a magnetic moment in an effective field. One usually starts from a general Landau–Lifshitz–Gilbert form [12,30] which in our notation reads

$$\frac{\mathrm{d}\boldsymbol{m}}{\mathrm{d}t} = -\gamma[\boldsymbol{m} \times \boldsymbol{h}_{\text{eff}}] - \alpha\left[\boldsymbol{m} \times \frac{\mathrm{d}\boldsymbol{m}}{\mathrm{d}t}\right], \tag{6}$$

where γ denotes the gyromagnetic ratio and α is a damping constant. This equation can be rewritten as

$$(1+\alpha^2)\frac{\mathrm{d}\boldsymbol{m}}{\mathrm{d}t} = -\gamma[\boldsymbol{m} \times \boldsymbol{h}_{\text{eff}}] - \tilde{\alpha}[\boldsymbol{m} \times [\boldsymbol{m} \times \boldsymbol{h}_{\text{eff}}]], \tag{7}$$

with $\tilde{\alpha} = \alpha\gamma$. The second term on the right in these equations was initially constructed to account for the energy dissipation and hence the solution of these equations should converge to the equilibrium magnetization configuration in the limit $t \to \infty$. If we are not interested in simulations of the remagnetization *dynamics* we can drop the first term and restrict ourself to the solution of the system of ordinary differential equations (ODE) of the form

$$\frac{\mathrm{d}\boldsymbol{m}_i}{\mathrm{d}t} = -\left[\boldsymbol{m}_i \times \left[\boldsymbol{m}_i \times \boldsymbol{h}_i^{\text{eff}}\{\boldsymbol{m}\}\right]\right], \tag{8}$$

where all constants have been absorbed into the reduced time t and the dependence of the effective field for each moment on the orientations of all other moments is explicitly indicated.

There exist a large variety of methods for solving ODE-systems like Eq. (8). The major goal of the most sophisticated of them such as predictor–corrector or Richardson extrapolation methods [22,23,31] is to allow for a maximal time step when certain accuracy requirements should be fulfilled. In our case the task is much simpler: we do *not* need to control the *accuracy* of our solution but merely have to maintain *stability* which means that we must only check that the system energy decreases after each 'time' step. For this reason we expect that usual Runge–Kutta-type (RK) methods should be good enough for finding an equilibrium magnetization configuration using Eq. (8).

Comparing the performance of Runge–Kutta methods of various orders we discovered that the time steps which various methods were able to take when the stability of the solution was required were roughly proportional to the order of the method. Because the number of the right-hand-side evaluations (which is obviously the most time-consuming part of the algorithm) is also approximately proportional to the method order, the time needed to obtain an equilibrium solution up to a certain accuracy (which is again given by the maximal rotation moment $\max(\|[\boldsymbol{m}_i \times \boldsymbol{h}_i^{\text{eff}}]\|)$ allowed) was approximately independent on the order of the method applied.

Such a behavior indicates that the corresponding ODE-system is 'stiff' [23,31] so that very small time steps are needed to maintain stability. Unfortunately, all methods developed especially for solving such stiff ODE-systems require the inversion of the system matrix for each time step. This inversion, being an $\sim L^3$-process for the $L \times L$ matrix, is absolutely

out of question in our case, where $L \sim 10^3$, what makes the application of corresponding methods impossible.

For this reason we have adopted the simplest possible explicit method – the Euler method with the following 'adaptive step-size control' [14]: when the energy after a certain time step Δt increases, we restore the magnetization configuration before this step and try again with the time step $\Delta t/2$. The process is repeated until the energy after this step decreases. To avoid unnecessary small time steps we try to double Δt if several (~ 10) steps with the same Δt have been successful (the energy dropped).

From the mathematical point of view this algorithm is closely related to the steepest descent method. The moment rotation in the effective field direction corresponds to movement in the direction of the local gradient if we remember that the magnitude of a moment should be constant. A decisive advantage of the algorithm described above is that only one function evaluation per iteration is required because we do not search for an energy minimum in the gradient direction. For the same reason a moment movement by the next iteration is not necessary perpendicular to its previous movement which also may lead to a faster convergence when moving along a 'curved valley floor'.

Eq. (7) also explains why we have chosen the convergence criterion in the form given above ($\|\boldsymbol{m}_i \times \boldsymbol{h}_i^{\text{eff}}\| < \epsilon$: only that component of the effective field which is perpendicular to the moment direction is 'responsible' for the movement of magnetic moment. For this reason it is enough to require small values of the vector product $\|\boldsymbol{m}_i \times \boldsymbol{h}_i^{\text{eff}}\|$ to assure that the magnetization state is close to the equilibrium.

The relaxation algorithm constructed this way was found to be significantly faster than conjugate gradients (see Fig. 4). A detailed analysis is again postponed till Section 2.5.

2.4. *'Alignment' methods*

The underlying idea for these methods is due to the basic assumption that magnetic moments can only be rotated (without changing their magnitude). This means that to obtain a (stable) equilibrium magnetization state it is sufficient to demand that each magnetic moment should be parallel to the effective field at the corresponding point. In such a state no further rotations of magnetic moments will occur, which can be seen also from Eq. (7) and Eq. (8) because in this case all vector products on the right-hand-side are exactly zero.

This insight leads to a following 'algorithm':

(s1) For the current magnetization state, evaluate $\boldsymbol{h}_i^{\text{eff}}$ for each moment.

(s2) Align each moment along the corresponding field.

(s3) Check whether the convergence criterion is met. If not, accept this new magnetization state and go to step (s1). If yes, we are done.

First suggestions concerning such 'alignment' algorithms can be found already in Ref. [12]. They were repeated in Refs. [27,32] and corresponding algorithms were partially used in Refs. [20,21]. However, it is quite evident that no scheme based on (s1)–(s3) only is likely to succeed in practice.

The simplest way to understand the reason for this is to realize that the algorithm (s1)–(s3) is nothing else but an attempt to solve a system of non-linear equations (below, $\hat{h}_{x,\alpha}$ denote components of a unit vector along the effective field: $\hat{\boldsymbol{h}} = \boldsymbol{h}_{\text{eff}}/h$)

$$\begin{cases} m_{x,i} = \hat{h}_{x,i}(\boldsymbol{m}), \\ m_{y,i} = \hat{h}_{y,i}(\boldsymbol{m}), \\ m_{z,i} = \hat{h}_{z,i}(\boldsymbol{m}) \end{cases} \tag{9}$$

substituting iteratively $m_{\alpha,i}^{(k+1)} = \hat{h}_{\alpha,i}(\boldsymbol{m}^{(k)})$, where $\{\boldsymbol{m}^{(k)}\}$ are magnetic moment unit vectors for the kth iteration. It is a textbook result that already in a 1D case the corresponding method for solving equations $x = f(x)$ (one simply puts $x^{(k+1)} = f(x^{(k)})$) converges if and only if $|\mathrm{d}f/\mathrm{d}x| < 1$ for the whole interval where we try to find a solution. There is obviously no reason why inequalities analogous to this one should hold in a general case for the system (9). Although the iteration process based on (s1)–(s3) can not diverge in our case because both $m_{\alpha,i}$ and $\hat{h}_{\alpha,i}$ are restricted ($m_i = \hat{h}_i = 1$), the algorithm can enter a nonconvergent cycle (what it really does).

However we found out that in all practical cases these cycles were very close to a simple oscillatory behavior (i.e., $\boldsymbol{m}^{(k)} \approx \boldsymbol{m}^{(k-2)}$) which enabled us to implement the following version of (s1)–(s3) to avoid

this oscillations. Instead of simply aligning each moment along the effective field, we build up a linear combination

$$\boldsymbol{m}_i^{(k+1)} = (1-\alpha_i)\,\boldsymbol{m}^{(k)} + \alpha_i \hat{\boldsymbol{h}}_i^{(k)} \qquad (10)$$

and normalize $\boldsymbol{m}_i$ after each iteration to satisfy the condition $m_i = 1$. Initially (for the first iteration at the new field value) all parameters $\alpha_i = 1$ which leads exactly to (s1–s3).

After performing an iteration step we store all moment moves $(\Delta \boldsymbol{m}_i)^{(k)} = \boldsymbol{m}_i^{(k+1)} - \boldsymbol{m}^{(k)}$. For the next iteration we reevaluate as usual the effective field using new moment orientations and try to move moments according to Eq. (10) with the same α-values. Then we check for each moment whether the two following conditions are fulfilled:

(i) the new proposed moment change $(\Delta \boldsymbol{m}_i)^{(k+1)}$ points approximately in the opposite direction relative to the previous one $(\Delta \boldsymbol{m}_i)^{(k)}$ (actually we check whether the angle between $(\Delta \boldsymbol{m}_i)^{(k+1)}$ and $(\Delta \boldsymbol{m}_i)^{(k)}$ exceeds $\pi/2$) *and*

(ii) the magnitude of the new proposed change is greater than or equal to the previous one $(|(\Delta \boldsymbol{m}_i)^{(k+1)}| \geq |(\Delta \boldsymbol{m}_i)^{(k)}|)$.

If both statements are true then we suspect that oscillatory behavior takes place, decrease α_i setting $\alpha_i \to \alpha_i/2$ and evaluate $(\Delta \boldsymbol{m}_i)^{(k+1)}$ again. We repeat this procedure for the given moment until one of the conditions (i) or (ii) is violated. Then we consider the proposed movement of the next moment etc.

Obviously the two checks (i) and (ii) allow to detect only the simplest oscillations of the kind $\boldsymbol{m}^{(k)} \approx \boldsymbol{m}^{(k-2)}$ and do not guard against cyclic behavior when one cycle involves several iterations. In our practice we never encountered such cycles. If there are any, a simple additional check that the energy decreases after all moments are moved can be used to ensure the convergence of the algorithm.

2.5. *Behavior of different methods for various single-particle anisotropy values*

Comparative analysis of the behavior of the three methods described above is presented in Fig. 4. Figs. 1–3b show the iteration number needed to achieve the equilibrium configuration for various field values starting from the magnetization state obtained in the previous field. In all figures corresponding remagnetization curves (upper parts of the hysteresis loops) together with the magnetic susceptibility are shown as part (a).

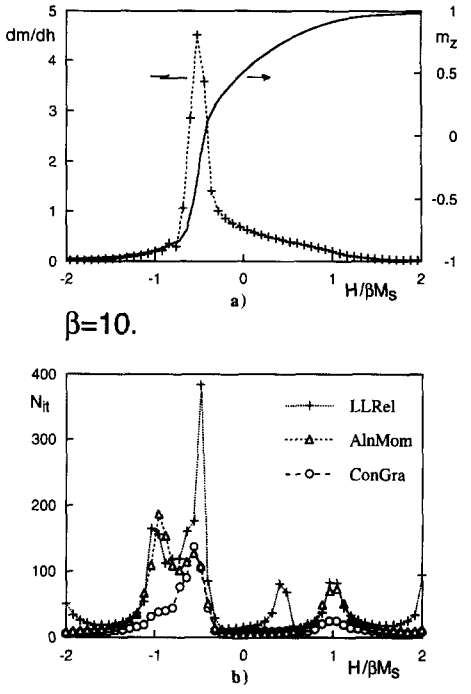

Fig. 1. Behavior of various numerical methods for $\beta = 10.0$. (a) Upper part of the hysteresis loop and the static magnetic susceptability, (b) iteration numbers required by the 'equation of motion' method (LLRel), 'alignment' method (AlnMom) and conjugate gradients (ConGra) to obtain an equilibrium state as functions of the external field.

All curves in Figs. 1–3 were obtained by averaging of simulation results for a system of $N = 256$ particles over 16 various spatial particle configurations. Particles were distributed randomly but non-overlapping with the volume concentration $\eta = 0.2$ inside a cube of a corresponding size. Periodical boundary conditions and demagnetizing tensor $\hat{D}$ corresponding to a spherical sample form were used by the evaluation of the interaction field via Eq. (3).

For all methods and anisotropy values the iteration number $N_{it}(h_z)$ as a function of the external field exhibits a peak which corresponds exactly to a peak in the magnetic susceptibility $\chi(h_z) = \mathrm{d}m/\mathrm{d}h_z$. Such a behavior is quite natural because larger χ value means larger magnetization change for the

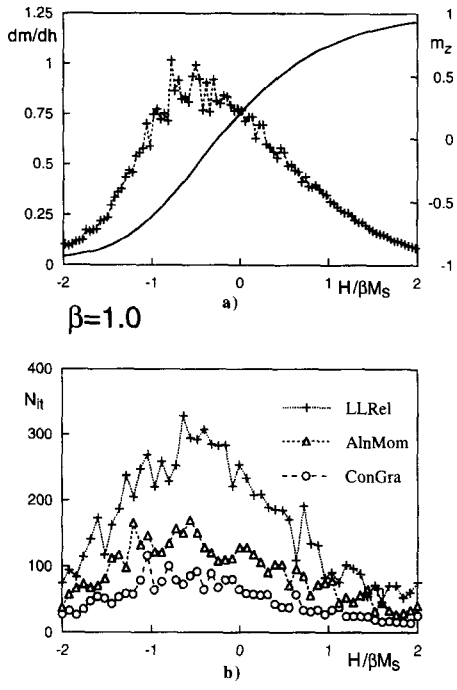

Fig. 2. The same as Figs. 1, 2 and 1 for the single-particle anisotropy value $\beta = 1.0$.

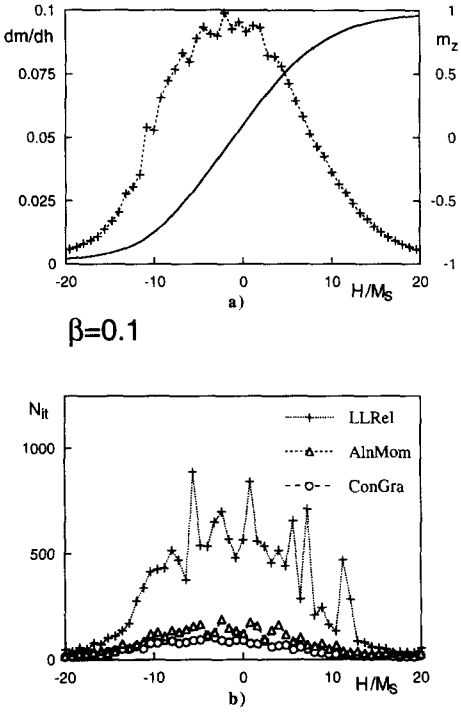

Fig. 3. The same as Figs. 3 and 1 for the single-particle anisotropy value $\beta = 0.1$.

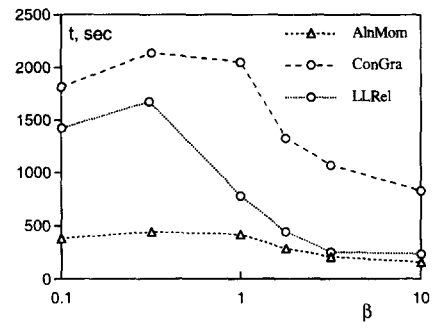

Fig. 4. Computation time (in seconds) required by various simulation methods (marked as in Figs. 1–3) to calculate a complete hysteresis loop (50 field values) for a system of 512 particles.

same external field decrement so that larger iteration number is required to equilibrate the system after the corresponding field change.

Additional peak for positive field $H_z/\beta M_s \approx 1.0$ which is present on the dependence $N_{it}(h_z)$ for the largest anisotropy value $\beta = 10.0$ signals a single particle behavior of the system for this anisotropy. Namely, it can be shown that if we neglect interaction effects then by $H_z^{ext}/\beta M_s \approx 1.0$ for particles with easy axis orientations $\theta \approx 0$ and $\theta \approx \pi/2$ the rotational moment acting on the magnetic moment near its equilibrium position is of the order $\sim (\Delta\psi)^2$ ($\Delta\psi$ is a small deviation from the equilibrium) instead of $\sim \Delta\psi$-dependence in a general case. This leads to a much slower convergence especially for the 'equation of motion'-method because the magnitude of the corresponding moment movements (see Eq. (8)) is proportional to this rotational moment. For the same reason the iteration number increases for this method by $h_z \approx 0.5$ (here the rotational moment is small for particles with $\theta \approx \pi/4$) and in the negative field $h_z \approx -1.0$ for all methods. Fortunately, as we shall see below, for large anisotropies a much faster random field approximation provides adequate results so that this slowing down is not really important.

For large and moderate anisotropy values $\beta \sim 1$–10 conjugate gradients method requires much less iterations than the two other methods. Unfortunately, each conjugate gradients iteration involves several function and gradient (energy and effective field) evaluations which results in a much larger computational time. Optimizing routines for the minimum

bracketing and 1D (linear) minimization given in Ref. [23] we achieved the averaged number of the function evaluation needed to bracket a minimum $\langle N_{br} \rangle \approx 4$ and to find a bracketed minimum $\langle N_f \rangle \sim 3$–5. This is quite close to the minimal possible values $N_{br}^{min} = 3$ and $N_f^{min} = 2$ so that we believe that no further decisive improvements of the conjugate gradients algorithm are possible.

Comparison of computational times needed by different methods to compute a complete hysteresis loop on the anisotropy constant β is given in Fig. 4. All times (in seconds) are obtained by the averaging over 16 spatial configurations of the 512-particle system with the particle volume concentration $\eta = 0.2$. Computations were performed on the HP-Workstation 712/60 with 32 Mb RAM and using the program code implemented in FORTRAN.

It can be seen that conjugate gradients need the largest computational time for the reasons explained above. Both equation-of-motion and alignment methods require only one effective field evaluation per iteration which greatly decreases the computational time. The alignment method has another advantage that the field reevaluation for the given particle can be done taking into account movements of other moments already performed during the current iteration (if the energy check is not carried out). This strongly reduces the iteration number needed and roughly doubles the convergence speed of the algorithm. For this reason this method has turned out to be the best one for all anisotropy values. For the most 'time-consuming' small anisotropies (because in this case collective remagnetization processes play a dominant role) the alignment method requires almost the same iteration number as the conjugate gradients do (see Fig. 3) and hence is 4–5 times faster due to a much smaller computational time per iteration.

Concluding this part of the paper we would like to discuss some acceleration possibilities for simulation methods listed above. In our opinion, the capacity of conjugated gradients for this system is practically exhausted. Large changes in the moment orientation during the remagnetization which can in principle take place for any field value cause this method to change the corresponding spherical coordinate system and to restart quite often (if any of the particle moments are in the dangerous vicinity of the polar axis). For this reason the application of conjugate gradients makes sense only when the system is already quite close to the final equilibrium state, but one needs an objective criterion to decide when it is the case.

For the 'equation-of-motion' methods the situation is quite different. Here some kind of 'trajectory extrapolation' methods which have proved to be quite successful in micromagnetics [33] can be applied. The idea behind these methods is to store moment coordinates during few subsequent iterations and consider these coordinate values as functions of the integration 'time'-moment 'trajectories'. These trajectories can then be extrapolated towards $t \to \infty$ and the minimum of the system energy as a function of the extrapolation 'time' along these trajectories can be found. A state obtained this way is then used as an initial state for the next few iterations to obtain 'trajectories' for the next extrapolation step etc.

This method was successfully applied to 'soft' micromagnetic problems where one needs many thousand iterations to achieve the equilibrium. For hysteresis loop simulations it is sufficient to consider systems with the moderate particle number $N \sim 10^3$ where the iteration number is about few hundreds. Hence here such extrapolation is not expected to be very efficient but the situation may change if we want to consider larger systems for simulations of magnetic recording processes. We would also like to mention quite a sophisticated combination of the 'equation-of-motion' and usual minimization methods which will be presented in Ref. [34].

Another possibility to accelerate both equation-of-motion and alignment methods arises from the fact that the interaction field is actually evaluated as a sum over the nearest neighbors only (see Eq. (3)). For this reason the system matrices both for the ODE-system (8) which is solved in the equation-of-motion methods and for the non-linear system (9) which is a basis of the alignment method are sparse. This means that their inversion can in principle be performed in $\sim N$ operation, N being a particle number. This, in turn, offers a possibility to apply backwards difference methods [31] to integrate the ODE-system (8) and Newton–Raphson-type methods to solve Eq. (9) [23]. However, the coefficient before $\sim N$ dependence in the operation number required for the inversion of sparse matrices with the

random pattern of non-zero elements is quite large, so that a decisive gain in the iteration number must be achieved for these methods to make them competitive with the standard methods described above.

We would like to point out here again, that the arguments presented above may be valid for the simulations of fine magnetic particle systems only, so that comparison of various simulation methods should be carried out for each new type of the micromagnetic problem.

3. Random field approximation and its validity

An alternative possibility to obtain magnetization curves for a fine particle system is the random field approximation (RFA). In this approximation any magnetic quantity of interest can be evaluated for a system of interacting particles as a convolution of the corresponding quantity for an ideal (non-interacting) system and the distribution density of the interaction field $\rho(h_{\text{int}})$. For example, the magnetization in the external field $\boldsymbol{h}_0$ can be calculated as

$$\boldsymbol{m}(h_{0z}) = \int \boldsymbol{m}^{(0)}(h)\,\rho(\boldsymbol{h}-\boldsymbol{h}_0)\,\mathrm{d}^3h, \qquad (11)$$

where $\boldsymbol{m}^{(0)}(\boldsymbol{h})$ denotes the magnetization of the ideal system.

We point out already here that in RFA all interparticle correlations – in our case correlations between particle magnetic moments – are neglected. Indeed, according to Eq. (11) the interaction field on each particle is considered as a random variable with some a priori known distribution density and hence the interaction field on the given particle is not correlated with the orientations of its magnetic moment and magnetic moments of its neighbors. For this reason we expect RFA to fail for low single-particle anisotropy values where collective remagnetization processes are especially important. But before finding out the validity region of RFA we have to calculate the interaction field distribution density required in Eq. (11).

3.1. Random field distribution density

Probably the first rigorous result concerning this problem is due to Anderson [35] who showed that the distribution of any interaction field component in a dilute system of aligned dipoles is a Lorentzian. This result was generalized in Ref. [36] for the system of dipoles with six allowed orientations (corresponding to possible orientations of OH^--defects in cubic KCl crystals [37]) and in Ref. [38] for dilute ensembles of small ferromagnetic particles the moments of which can have any orientation.

On the other hand, basing on the numerical simulation results, Fähnle [19,39] claimed that for amorphous binary alloys $A_{1-x}B_x$ where only atoms A carry a dipole moment the interaction field distribution $\rho(h)$ is Gaussian for all x in the system with aligned moments [19] and for large concentration of magnetic atoms for randomly oriented dipoles [39]. To decide whether the distribution is a Gaussian one Fähnle used the ratio $F/\sqrt{2\sigma^2}$ of the distribution function area F (normalized so that $\rho(0)=1$) to the field dispersion σ^2 which for the Gaussian distribution should be $F/\sqrt{2\sigma^2}=\sqrt{\pi}$. Though this criterion is clearly insufficient to find out whether the studied distribution is indeed Gaussian (one can construct infinitely many distributions satisfying this relation but having entirely different distribution densities), results listed in Ref. [39] indicate some systematic change of $\rho(h)$ by decreasing x.

Hence the problem which should be solved concerns the behavior of the interaction field distribution when the particle concentration increases. In this section we demonstrate that with increasing concentration this distribution transforms from the Lorentzian to the Gaussian one. Furthermore, we show that spatial correlations of particle positions due to the excluded volume effect (particles should not overlap) significantly influence the distribution width already for moderate volume concentrations $\eta \sim 0.1$. And finally we demonstrate that in systems with aligned moments *angular* position correlations for particles which form the first coordination sphere around the trial particle strongly reduce the distribution width.

The dipole field created by a single particle $\boldsymbol{h}^{\text{sp}}$ located at the coordinate origin is

$$\boldsymbol{h}^{\text{sp}}(\boldsymbol{r}) = V_{\text{p}}\frac{3\boldsymbol{e}_{\text{r}}(\boldsymbol{e}_{\text{r}}\boldsymbol{m})-\boldsymbol{m}}{r^3} \equiv V_{\text{p}}\frac{\tilde{\boldsymbol{h}}(\boldsymbol{e}_{\text{r}})}{r^3}. \qquad (12)$$

Neglecting all spatial correlations in positions of other particles with respect to the trial one except the

restriction $r \geq r_{\min} = 2a$, we can easily obtain the interaction field dispersion $\sigma^2_{\alpha\beta} = \langle h_\alpha h_\beta \rangle$ for the system with the particle volume fraction η [38] (α, $\beta = x, y, z$):

$$\sigma^2_{\alpha\beta} = NV_p^2 \int_{2a}^{\infty} \frac{\langle \tilde{h}_\alpha(\boldsymbol{e}_r)\tilde{h}_\beta(\boldsymbol{e}_r)\rangle}{r^6} d^3r$$

$$= \frac{2\pi^2\eta}{15}\left\{\delta_{\alpha\beta} + \frac{\langle m_\alpha m_\beta\rangle}{3}\right\}. \quad (13)$$

To evaluate the distribution $\rho(h_\alpha)$ itself we apply the standard Margenau method [38,40,41] which uses the definition of $\rho(h_\alpha)$ as

$$\rho(h_\alpha) = \int_{r>2a} P(\{\boldsymbol{r}_i\})\delta\left(h_\alpha - \sum_{i=1}^{N} h_\alpha^{sp}(\boldsymbol{m}_i, \boldsymbol{r}_i)\right) \times \prod_{i=1}^{N} d^3r_i, \quad (14)$$

where $P(\{\boldsymbol{r}_i\})$ denotes the probability density to find the ith particle at the point $\boldsymbol{r}_i$ if the trial particle is placed at the coordinate origin. For the dilute system when all spatial correlations can be neglected, $P(\{\boldsymbol{r}_i\}) = 1/V^N$ (V is the system volume). Using the well known integral representation of the δ-function, the Fourier transform of, for example, $\rho(h_z)$ can be rewritten in the limit $V \to \infty$ via the one-particle integral [35,38,41]

$$I(k_z) = 1 - \frac{1}{V}\left\langle \int \left[1 - \exp(-ik_z h_z^{sp}(\boldsymbol{m}, r))\right] d^3r \right\rangle \quad (15)$$

as $F(k_z) = I(k_z)^N$. For large $k_z \gg k_{\min} (\sim 1)$ the explicit evaluation of Eq. (15) gives $I = |k_z| A(\boldsymbol{m}) V_p/V$, where the function $A(\boldsymbol{m})$ can be calculated numerically and shows only a weak dependence on the magnetic moment orientation [38]. This $\sim |k_z|$-dependence of I leads directly to the Lorentzian form of $F(h_\alpha)$ [35,38,41] since in this case its Fourier transform is $F(k_z) = I(k_z)^N \sim \exp(-|k_z| NV_p/V) \equiv \exp(-\eta|k_z|)$.

The assumption $k \gg k_{\min}$ means that the Lorentzian distribution obtained this way is valid for $h \ll h_{nn}$, where h_{nn} denotes the field created by the single nearest neighbor ($r_{\min} = 2a$), so that some cut-off should be introduced by large field values [38]. For most applications it is sufficient to take $\rho(h_z)$ in the form

$$\rho(h_z) = \frac{C_N}{1 + (h_z/\Delta)^2}, \quad |h_z| \leq h_c, \quad (16)$$

and $\rho(h_z) \equiv 0$ for $|h_z| > h_c$. Here C_N denotes the normalization constant and $\Delta \approx 4.54\eta$ [38] is the distribution width. The cut-off value h_c should be determined from the condition $\langle h_z^2 \rangle = \sigma_{zz}^2$ which ensures that the distribution (16) has the correct dispersion (Eq. (13)).

For dilute systems ($\eta \ll 1$) the condition $h \ll h_{nn}$ holds for almost the whole field region of interest, because the probability to find even one neighbor on the distance $r \sim r_{\min} = 2a$ is very small. But by increasing the volume concentration this condition is violated for most particles for two reasons: (i) the mean interparticle distance $\bar{r}$ tends to the minimal distance $2a$ and (ii) spatial correlations in the particle positions become important, so that the assumption $P(\{\boldsymbol{r}_i\}) = 1/V^N$ is no longer valid.

The simplest possible way to take these spatial correlations into account is to include pair correlations only introducing the pair distribution function (PDF) [42] $g(r)$ into Eq. (15):

$$I(k_z) = 1 - \frac{1}{V}\left\langle \int \left[1 - \exp(-ik_z h_z^{sp}(\boldsymbol{m}, \boldsymbol{r}))\right] \times g(r) d^3r \right\rangle. \quad (17)$$

Already for a moderate volume concentration ($\eta \sim 0.1$) $g(r)$ starts to exhibit a peak for $r \approx 2a$ signalling the formation of a short-range-order: the first coordination sphere (see, e.g., Ref. [42], chapter 2). This means that the probability to find a neighboring particle at the distance $r = r_p \approx 2a$ is strongly enhanced, which results in the increase of the interaction field.

A quite large maximal number of the nearest neighbors $N_{\max} = 12$ (achieved for the perfect hexagonal lattice) together with the trend $\bar{r} \to r_{\min} = 2a$ mentioned above allows us to assume that for sufficiently high volume concentration η the opposite assumption $|h_z| \gg h_{nn}$ is valid for most particles. Hence we can expand the exponent in Eq. (17) up to the second order in the small quantity $k_z h_z^{sp}$ ($k_z \sim$

$1/h_z \ll 1/h_z^{sp}$). Then the real part of Eq. (17) takes the form

$$I(k_z) = 1 - \frac{1}{2V}\left\langle \int [k_z h_z^{sp}(\boldsymbol{m},\boldsymbol{r})]^2 g(r) \mathrm{d}^3 r \right\rangle, \quad (18)$$

so that $F(k_z) = I^N(k_z^2$, which immediately leads to the Gaussian distribution $\rho(h_z)$ with the dispersion

$$\sigma_z^2 = \frac{4\pi}{3}\eta \int_{2a}^{\infty} \frac{g(r)\,\mathrm{d}r}{r^4} \int_{\Omega} \tilde{h}_z^2(\boldsymbol{m})\,\mathrm{d}\Omega_{\boldsymbol{m}}. \quad (19)$$

The reasons given above are nothing else but the statement that the number of particles M essentially contributing to the interaction field on the given particle is large ($M \gg 1$), so that the central limit theorem can be applied for the evaluation of $\rho(h_\alpha)$. As it can be seen, the dispersion (19) coincides with Eq. (13) except that the PDF $g(r)$ is introduced.

To check whether the interaction field distribution for higher particle concentrations becomes indeed Gaussian, we performed direct numerical simulations. For each volume concentration 50 configurations each consisting of 2048 particles were generated choosing particle positions randomly but non-overlapping. Then the interaction field on each particle was calculated using Eq. (3) and assuming periodical boundary conditions and zero demagnetizing field. Simulations were performed for two limiting cases of randomly oriented and fully aligned particle moments. Method to generate random fields with a distribution corresponding to the arbitrary orientation degree of magnetic moments is discussed below where a concrete implementation of RFA for hysteresis loop calculations is described.

In Fig. 5 two histograms of simulated distributions (for low and high particle volume concentrations) for systems with randomly oriented moments are compared with (i) Gaussian distributions with dispersions (19) (solid line) and (ii) the restricted Lorentzian distribution (Eq. (16)). It can be seen, that for $\eta = 0.01$ the simulated $\rho(h_z)$ coincides with the corresponding Lorentzian, whereas for $\eta = 0.25$, with the Gaussian distribution confirming the assumption that $\rho(h_z)$ transforms from the Lorentzian to the Gaussian distribution with increasing particle concentration. As a quantitative criterion of the difference D between the simulated $\rho_{sim}(h_\alpha)$ and the

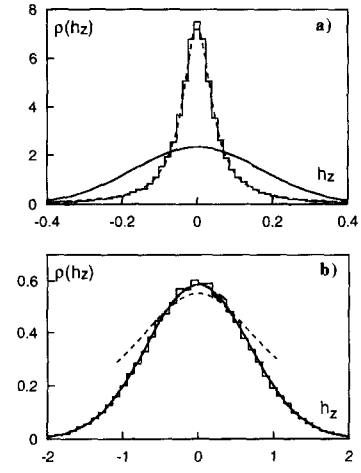

Fig. 5. Distribution densities $\rho(h_z)$ of the z-projection of the interaction field for particle volume fractions $\eta = 0.01$ (a) and $\eta = 0.25$ (b). Histograms – numerical simulation results, solid lines – Gaussian distributions with the same dispersion, dotted lines – restricted Lorentzian distributions (16).

Gaussian $\rho_G(h_\alpha)$ distributions we have used the integrated absolute value of their difference

$$D = \int_{-\infty}^{\infty} |\rho_{sim}(h_\alpha) - \rho_G(h_\alpha)| \mathrm{d}h_\alpha. \quad (20)$$

In our case the mean of the corresponding Gaussian distributions ($\bar{h}_\alpha = 0$) is known in advance, whereas its dispersion is obtained from the simulated data. Values of D for $\rho(h_z)$ are shown in Fig. 6a as a function of the particle concentration η for randomly oriented (triangles) and aligned (crosses) dipole moments. With increasing particle concentration the simulated distribution converges to the Gaussian more rapidly for the randomly oriented system, which is obviously due to the additional disorder arising from the random orientation of dipole moments in comparison with the aligned system.

To find out, for which concentrations the difference between the simulated and the Gaussian distributions are statistically significant, we applied the ω^2-criterion [43]. It allows to calculate the probability that the difference between the known distribution function (Gaussian in our case) and the distribution function derived from some empirical data set exceeds some prescribed value if the distribution law of these data is indeed Gaussian.

The dependencies of ω^2-values on the particle volume fraction η are shown in Fig. 6b for randomly oriented (triangles) and aligned (crosses) dipoles. The horizontal line represents the probability level $P = 95\%$, which for the ω^2-criterion calculated using the Gaussian distribution with the dispersion derived from the empirical data is $\omega^2(P = 0.95) = 0.442$ [43]. All ω^2-values greater than this one should, strictly speaking, lead to the conclusion that the studied distribution is *not* Gaussian, i.e., deviations from the Gaussian distribution are statistically significant. It can be seen that for randomly oriented moments the distribution can be treated as Gaussian for $\eta \geq 0.2$, whereas for aligned moments small (see Fig. 6a), but statistically significant deviations from the Gaussian distribution occur up to the highest concentration $\eta = 0.35$ available by such simulations.

For the Lorentzian distribution it was impossible to perform the same ω^2-test for all concentrations except the smallest ones ($\eta < 0.03$), where the distribution is clearly Lorentzian. The reason is that the analytical form (16) does not describe the distribution tails correctly leading to wrong values of the ω^2-criterion which is very sensitive to such details.

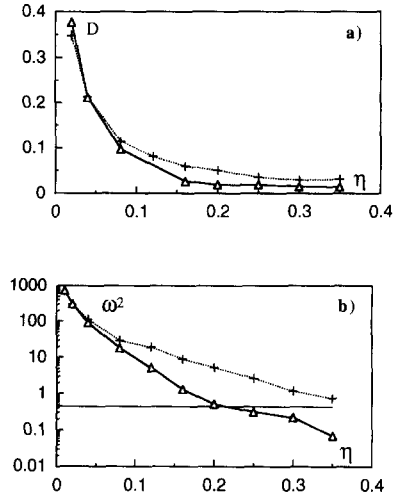

Fig. 6. (a) Integrated differences D (Eq. (20)) between the simulated and the corresponding Gaussian distribution densities and (b) values of the ω^2-criterion (calculated to check whether the distribution obtained numerically is a Gaussian one) as functions of the particle volume fraction η for randomly oriented (triangles) and aligned (crosses) moments. ω^2-values above the horizontal line (corresponding to the 95% probability level) indicate statistically significant deviations from the Gaussian distribution.

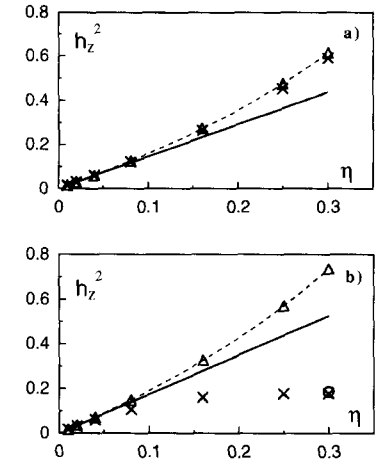

Fig. 7. Interaction field dispersion $\overline{h_z^2}$ as function of the particle volume fraction η for randomly oriented (a) and aligned (b) dipoles. Crosses – numerical simulation values, solid lines – ideal dependencies (Eq. (13)), triangles – values calculated from Eq. (19), i.e., taking into account radial correlations only. Dashed lines through triangles are the guide for the eye. The open circle on (b) represents the value obtained for $\eta = 0.3$ when perfect short-range order is assumed (see text for details).

We also found that the dispersion of the interaction field distribution strongly depends on the orientation degree of the particle moments. In Fig. 7 dependencies $\overline{h_z^2}(\eta)$ obtained using different methods are shown for randomly oriented (Fig. 7a) and aligned (Fig. 7b) dipoles. Crosses indicate values obtained by numerical simulations, straight solid lines represent linear dependencies (13) which neglect all spatial correlations except the condition $r \geq 2a$ and open triangles stand for $\overline{h_z^2}$-values obtained by Eq. (19), i.e., taking into account radial pair correlations only. The corresponding PDF $g(r)$ was accumulated for all configurations obtained during numerical simulations. It can be seen that the latter approach provides good agreement with the numerical simulation results for the randomly oriented dipoles (Fig. 7a), whereas for the aligned system (Fig. 7b) it fails to predict even the correct trend of the $\overline{h_z^2}(\eta)$-dependence when compared with the ideal case (straight line). This behavior differs also from the corresponding dependence in RKKY spin glasses, where $\overline{h_z^2}$ was

found to be larger for the aligned system than for the chaotic one [44].

We assumed, that for the aligned system $\overline{h_z^2}$ is strongly reduced due to the *angular* correlations of the *positions* of particles forming the first coordination sphere around the trial particle. Fields of these particles make the dominant contribution to $\overline{h_z^2}$ and correlations of their angular positions would reduce $\overline{h_z^2}$ for the aligned system because the only disorder left in this case is due to the random orientation of this first coordination shell relative to the given particle. To test this assumption we calculated $\overline{h_z^2}$ for $\eta = 0.3$ assuming that the nearest neighbors of the trial particle form the perfect hexagonal shell and the positions of other neighbors are uncorrelated except that they are outside this shell ($r > 4a$). To compute the contribution to $\overline{h_z^2}$ from this hexagonal shell we performed numerical averaging over its possible orientations given by the corresponding Euler angles. The result (total $\overline{h_z^2}(\eta = 0.3) \approx 0.189$) is shown in Fig. 7b by the open circle. It is in a good agreement with the value $\overline{h_z^2}(\eta = 0.3) \approx 0.179$ obtained numerically.

Another interesting feature of the aligned system is a substantial skewness (third moment) of the h_z-component distribution for low particle concentrations (z-axis is chosen along the aligned dipoles). The dependence of this quantity defined as

$$s = \int_{-\infty}^{\infty} h_z^3 \rho(h_z)\, \mathrm{d}h_z \qquad (21)$$

on the particle volume fraction $s(\eta)$ is shown in Fig. 8. We point out that this skewness is a consequence of a h_z-distribution shift which is due *not* to the demagnetization but to the non-zero imaginary part of the one-particle integral (15) as it was mentioned in Ref. [38].

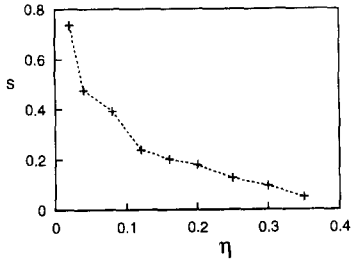

Fig. 8. Skewness of the distribution density $\rho(h_z)$ for the aligned system as a function of the particle volume fraction η.

In conclusion, in this section we have shown that in the disordered fine magnetic particle system the distribution density of the dipolar interaction field transforms from the Lorentzian to the Gaussian form when the particle volume fraction η increases. The transition for randomly oriented magnetic moments is completed by $\eta \approx 0.2$, whereas for the aligned system even for the highest studied particle volume fraction $\eta = 0.35$ statistically significant deviations from the Gaussian distribution still exist. Already for moderate particle concentrations $\eta \geq 0.1$ the interaction field dispersion is strongly influenced by the radial and – for systems of aligned dipoles – angular correlations of the particle positions, so that these correlations should be explicitly taken into account.

3.2. RFA calculations of the magnetization curves

Calculating any magnetization curve in the random field approximation is a straightforward task which involves 'only' the proper evaluation of the integral (11) for given system parameters. Unfortunately, corresponding ideal magnetization dependencies can be obtained only numerically even in the simplest case of the uniaxial single-particle anisotropy [45]. This means that integral (11) can not be evaluated analytically even if the interaction field distribution density is approximated good enough by some ananlytical function (restricted Lorentzian or Gaussian form for low and high particle concentrations correspondingly).

For this reason we calculated hysteresis loops by the Monte-Carlo evaluation of (11). To generate an interaction field distribution for arbitrary particle concentration we have applied the following method. As for real simulations, a random but non-overlapping particle configuration with randomly oriented anisotropy axis was generated. Using the magnetization state obtained in the previous field value (the saturated state for the first field), we evaluated the interaction field on each particle via Eq. (3). Then these interaction fields were 'redistributed' randomly between particles, i.e., a dipole field acting on the ith particle was set to $\boldsymbol{h}_j^{\mathrm{int}}$, where $j \neq i$ was chosen randomly. This way an interaction field distribution corresponding to the given average orientation de-

gree of magnetic moments was generated whereby the interaction field acting on each particle was not correlated with its position and orientation of its magnetic moment as it is required by Eq. (11).

The interaction field distribution obtained with the method described above contains a systematical error due to the fact that this distribution depends on the average orientation degree of magnetic moments which changes with the field. For this reason the interaction field distribution obtained from the magnetization state achieved in the previous field is not exactly the same as for the current field value. But if the field decrement is sufficiently small this error can be neglected.

After generating all interaction fields an equilibrium moment orientation for each particle was found using the iteration procedure analogous to the alignment method described above. It works in this case extremely fast because we do not need to reevaluate interaction fields for each iteration. In fact, corresponding equilibrium orientation angles can be tabulated in advance for the given anisotropy value as a function of the easy axis orientation and the total field (which in this case would be a sum of the external field and (random) interaction field). This table can then be used to evaluate an equilibrium magnetic moment orientation for any direction of a particle easy axis and any value of an interaction field encountered by simulations using a simple interpolation procedure. This trick would result in further acceleration of such RFA calculations but we did not use it because the computational effort to obtain hysteresis loops with the accuracy better than 1% using RFA was negligible even when the iterative alignment procedure was used.

3.3. Validity region of the RFA

To find out, for which particle anisotropies β and volume concentrations η RFA provides adequate results by hysteresis loop calculations we have performed such calculations for particle systems with single-particle anisotropy constants $0.0 \le \beta \le 10.0$ and particle volume fractions $0.01 \le \eta \le 0.32$ using RFA and compared it with the results of 'real' simulations carried out using the alignment method. As a measure of the error introduced by the RFA we have chosen an integrated difference between hysteresis loops computed using RFA and 'real' simulations normalized on the hysteresis loop area:

$$\delta = \frac{\int_{-\infty}^{\infty} |m_z^{\mathrm{RFA}}(h_z) - m_z^{\mathrm{al}}(h_z)| \mathrm{d}h_z}{\int_{-\infty}^{\infty} |m_z^{\mathrm{al}}(h_z) + m_z^{\mathrm{al}}(-h_z)| \mathrm{d}h_z} = \frac{1}{S_{\mathrm{hyst}}} \int_{-\infty}^{\infty} |m_z^{\mathrm{RFA}}(h_z) - m_z^{\mathrm{al}}(h_z)| \mathrm{d}h_z. \quad (22)$$

Values of this relative differences were evaluated from hysteresis loops simulated with the 'alignment' algorithm and calculated using the RFA (11) for all (β,η)-pairs for the following parameter values: $\beta =$ 0.0, 0.1, 0.18, 0.32, 0.56, 1.0, 1.78, 3.16, 5.62, 10.0 (this choice corresponds to equidistant points on the logarithmic β-scale) and $\eta = 0.01$, 0.02, 0.04, 0.08, 0.12, 0.16, 0.20, 0.24, 0.32. For each (β,η)-pair a complete hysteresis loop with magnetization computed for 50 h_z-values was evaluated for 16 various random spatial configurations of a system of 1024 particles and an averaging of all measured quantities over these 16 configurations was performed.

A mesh plot $\delta(\beta,\eta)$ is presented in Fig. 9a. For those (β,η) values for which this quantity is small

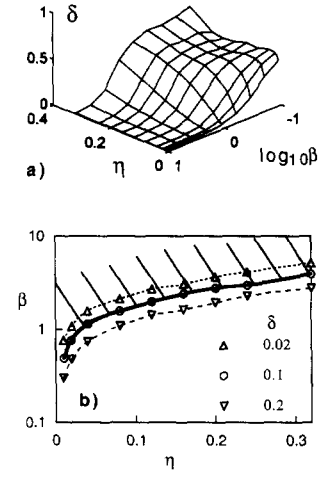

Fig. 9. (a) Mesh plot of the integrated relative difference δ (Eq. (22)) between hysteresis loops calculated using RFA and 'real' simulations as a function of the particle volume fraction η and anisotropy β. (b) contour lines of the mesh plot of Fig. 9a corresponding to δ-values shown on the picture. Dashed area represents the (β,η) region where the random field approximation is valid.

($\delta \ll 1$) the random field approximation can be considered as valid and used by the numerical treatment of quasistatic remagnetization processes as a much faster alternative to 'real' simulation methods. Contour lines on the (β,η)-plane corresponding to the difference values $\delta = 0.02$, 0.1, 0.2 are shown in Fig. 9b (note the logarithmic scale on the β-axis). If we consider a relative difference of 10% ($\delta = 0.1$) as acceptable then the dashed area in Fig. 9b represents the validity region of the random field approximation. It can be seen that for higher particle concentrations larger anisotropy values are required to make RFA valid.

This diagram has also an important physical sense because it can be viewed as a 'phase diagram' showing the regions on the anisotropy–concentration plane where either single-particle or collective remagnetization processes dominate. Indeed, the major RFA-assumption that the interaction field is not correlated with the particle position and its magnetic moment orientation (see above) means that all collective remagnetization processes are neglected. Hence the failure of the RFA signals the establishing of the collective remagnetization behavior so that the solid line in Fig. 9b can be considered as a 'phase boundary' on the (β,η)-plane above which the single-particle and below the collective behavior dominates remagnetization processes in fine-particle systems with the uniaxial single particle-anisotropy. Only below this line a collective spin-glass-like behavior (may be, a phase transition to a 'frozen' state by decreasing a temperature) can be expected. This diagram, hence, is analogous to the phase diagram mentioned (but unfortunately not shown) in Ref. [46].

4. Physical results

4.1. Hysteresis loops

A typical set of hysteresis loops for various anisotropy values for a given particle concentration ($\eta = 0.16$) is shown in Fig. 10. For the highest anisotropy values studied (see Fig. 10a) $\beta = 10.0$ and $\beta = 5.62$ the loops for an interacting system are very close to ideal hysteresis loops for a non-interacting Stoner–Wohlfarth model (see, i.e., [38,45])

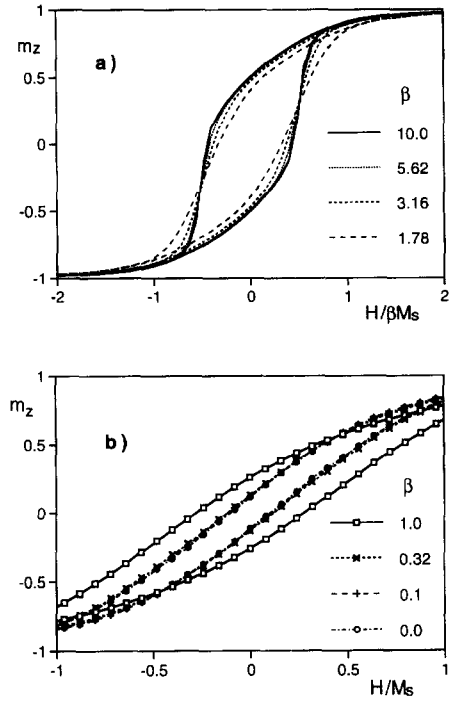

Fig. 10. Typical hysteresis loops for $\eta = 0.16$ for large (a) and small (b) values of the single-particle anisotropy β. Only central part of the calculated loops is shown on (b) to enhance resolution.

because for high single-particle anisotropy practically the only effect of the interparticle interaction is to remove a square-root singularity in the static magnetic susceptability of a system [38].

For intermediate anisotropy values interaction effects gradually became more and more important (see loops for $\beta = 3.16$, 1.78, 1.0). Finally, for small anisotropies (Fig. 10b, note another scaling of the field axis) these effects completely determine the hysteretic behavior of the system what can be seen from the fact that for $\beta < 0.32$ hysteresis loops do not depend on the concrete anisotropy value and practically coincide with the loop obtained for isotropic particles ($\beta = 0$, see Fig. 10b). This hysteresis due to the collective interparticle interaction effects was found in [20] and its existence was later confirmed in [25,29].

4.2. Remanence and coercivity

Two most important parameters of the hysteresis loop – reduced remanence $j_R = m_z(h_z = 0)$ and coercivity h_c (such a field that $m_z(-h_c) = 0$) are

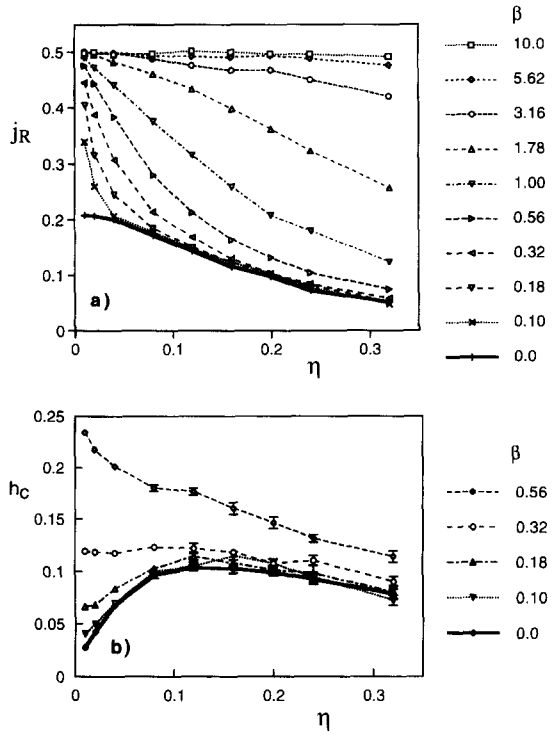

Fig. 11. Concentration dependencies $j_R(\eta)(a)$ and $h_c(\eta)$ for various anisotropy values indicated in the figures.

shown as functions of particle anisotropy β and particle volume concentration η in Fig. 11.

It can be seen that for large anisotropy values β the remanence j_R depends on the particle concentration η only slightly (Fig. 11a) and its value is very close to the remanence of an ideal (non-interacting) system of particles with a uniaxial magnetic anisotropy and a chaotic distribution of easy axes $j_R^{(0)} = 0.5$. For very low anisotropy values (Fig. 11a) the $j_R(\eta)$ dependence approaches the limiting curve for $\beta = 0$ when the concentration increases. We also mention, that in this case of the Stoner–Wohlfarth system with randomly oriented anisotropy axes the difference between the measured j_R and the ideal value $j_R^{(0)} = 0.5$ can also be used for building up a phase diagram showing regions of a single-particle and collective behavior but the criterion Eq. (22) is more general.

The coercivity for large anisotropies also depends on the particle concentration only slightly and is again very close to the ideal Stoner–Wohlfarth value $h_c \approx 0.48\beta$ [45]. The decrease of h_c with growing particle concentration for large anisotropy values results from the influence of the effective field fluctuations due to the interparticle interactions. Such fluctuations always reduce the number of metastable states in a system where these states result from a single-particle anisotropy effects [42].

The most interesting feature of the system is a non-monotonic concentration dependence of the coercivity $h_c(\eta)$ for small anisotropies where h_c is determined entirely by the interaction effects (Fig. 11b). The coercivity maximum occurring near $\eta \approx 0.15$ is quite flat but clearly beyond 'measurement' errors. A possible explanation of this behavior can be given as follows. When the particle concentration increases starting from very small values the interaction effects responsible for the hysteretic behavior (by small single-particle anisotropy values) became more pronounced leading to the initial increase of $h_c(\eta)$-dependence. But when the concentration increases further, a short-range spatial order is formed so that 'a degree of disorder' reduces for larger concentrations leading to the decrease of h_c (hysteresis is absent for a fully ordered particle system at least for cubic and hexagonal lattices).

We point out, that the decrease of h_c for large concentrations can *not* be attributed to the reduction of the local field fluctuations because the latter grow monotonically with η which is demonstrated by the concentration dependence of the local field dispersion (Fig. 8). This is another evidence that the single-particle picture when used for small anisotropy values lead to *qualitatively* wrong conclusions.

This result can be directly compared only with $h_c(\eta)$-dependence obtained by Zhao and Bertram [29] who also performed numerical simulations of hysteresis loops for ordered and disordered systems of particles without intrinsic anisotropy. The dependence $h_c(\eta)$ presented in Ref. [29] shows somewhat smaller coercivity values for $\eta > 0.1$ and a saturation of $h_c(\eta)$ when the particle concentration increases. We attribute both differences to a much smaller number of particles for systems simulated in Ref. [29]. The system size is especially important for large particle volume fractions where local fluctuation effects became stronger so that an averaging over larger systems and greater configuration number is necessary to obtain sufficiently accurate results.

5. Conclusion

We have presented a detailed numerical study of the Stoner–Wohlfarth model including interparticle interaction effects in a wide range of particle volume concentrations and single-particle anisotropy values. Among various methods used for numerical simulations of this system the alignment method is shown to be the fastest especially in the physically most interesting region of small single-particle anisotropies.

A random field approximation is analyzed. It is shown that the distribution density of the interaction field required to perform any calculations within this approximation transforms from a Lorentzian to a Gaussian one when the particle volume concentration increases. The region of concentration–anisotropy values where the RFA provides adequate results by simulations of quasistatic remagnetization processes is found.

Hysteresis loops for particle volume concentrations $0.01 \leq \eta \leq 0.32$ and single particle anisotropies $0 \leq \beta \leq 10.0$ are calculated. Dependencies of the coercivity and remanence on these parameters $h_c(\eta,\beta)$ and $j_R(\eta,\beta)$ are given. In particular, it is shown that for very small anisotropies the $h_c(\eta)$-dependence is non-monotonic.

Acknowledgements

The author would like to thank participants of the seminar of Prof. P. Görnert (IPHT Jena, Germany) for useful discussion, and Prof. W. Andrä for carefully reading the manuscript. Financial support of the Deutsche Forschungsgemeinschaft is greatly acknowledged.

References

[1] Magnetic Properties of Fine Particles, eds. J.L. Dormann and D. Fiorani (North-Holland, Amsterdam, 1992).
[2] K. O'Grady, IEEE Trans. Magn. 26 (1990) 1870.
[3] G.A. Pankhurst and R.J. Pollard, J. Phys. Condens. Matter 5 (1993) 8487.
[4] H. Bertram, IEEE Trans. Magn. 22 (1986) 460.
[5] A. Bradbury, S. Menear and R.W. Chantrell, J. Magn. Magn. Mater. 54–57 (1986) 745.
[6] K. Binder and A.P. Young, Rev. Mod. Phys. 58 (1986) 801.
[7] D.H. Reich, T.F. Rosenbaum and G. Aeppli, Phys. Rev. Lett. 59 (1987) 1969.
[8] D. Fiorani, J. Phys. C (GB) 19 (1986) 5495.
[9] D. Walton and D.J. Danlop, Solid State Commun. 53 (1985) 359.
[10] V.S. Dotsenko, Physics Usp. (USA) 36 (1993) 455.
[11] D. Wei, H.N. Bertram, A. Friedmann and R.H. Dee, IEEE Trans. Magn. 31 (1995) 2898.
[12] W.F. Brown, Micromagnetics (John Wiley, New York, 1963).
[13] S.W. Yuan and H.N. Bertram, IEEE Trans. Magn. 28 (1992) 2031.
[14] D.V. Berkov, K. Ramstoeck, A. Hubert, Phys. Status Solidi (a) 137 (1993) 207.
[15] D.R. Fredkin and T.R. Koehler, IEEE Trans. Magn. 24 (1988) 2362.
[16] D.R. Fredkin, T.R. Koehler, IEEE Trans. Magn. 25 (1989) 3473.
[17] J. Ehlert and W. Sperber, Phys. Status Solidi (a) 116 (1989) 389.
[18] D.V. Berkov, J. Magn. Magn. Mater. 99 (1991) L7.
[19] M. Fähnle, J. Magn. Magn. Mater. 15–18 (1980) 133.
[20] D.V. Berkov and S.V. Meshkov, IEEE Trans. Magn. 26 (1990) 1804.
[21] M.J. Vos, R.L. Brott, J. Zhu and L.W. Carlson, IEEE Trans. Magn. 29 (1993) 3652.
[22] F.S. Acton, Numerical Methods That (Usually) Work (Math. Ass. of America, Washington, DC, 1990).
[23] W.H. Press, S.A. Teukolsky, W.T. Vettrling, B.P. Flannery, Numerical Recipes in FORTRAN: the Art of Scientific Computing (Cambridge University Press, 1992).
[24] W. Williams and D.J. Dunlop, Phys. Earth Planetary Interior 65 (1990) 1.
[25] D.R. Fredkin, W. Chen and T.R. Koehler, IEEE Trans. Magn. 28 (1992) 2880.
[26] Y. Nakatani and Y. Uesaka, Jpn. J. Appl. Phys. 128 (1989) 2485.
[27] H. Bertram and H. Schabes, J. Appl. Phys. 64 (1988) 1347.
[28] S.W. Yuan and H. Bertram, Phys. Rev. B 44 (1991) 12395.
[29] Y. Zhao and H.N. Bertram, J. Magn. Magn. Mater. 114 (1992) 329.
[30] H.-B. Braun, Phys. Rev. B 50 (1994) 16501.
[31] C.W. Gear, Numerical Initial Value Problems in Ordinary Differential Equations (Englewood Cliffs, Prentice-Hall, 1971).
[32] E. Della Torre, J. Appl. Phys. 67 (1990) 5370.
[33] D. Berkov, K. Ramstoeck, T. Leibl and A. Hubert, IEEE Trans. Magn. 29 (1993) 2548.
[34] K. Ramstoeck, W. Hartung and A. Hubert, to be published in Phys. Status Solidi (a).
[35] P. Anderson, Phys. Rev. 82 (1951) 342.
[36] M.W. Klein, C. Held and E. Zuroff, Phys. Rev. B 13 (1976) 3577.
[37] V. Kuhn and F. Lüty, Solid State Commun. 2 (1964) 281.
[38] D.V. Berkov and S.V. Meshkov, Sov. Phys JETP 94 (1988) 140.
[39] M. Fähnle, Appl. Phys. 23 (1980) 267.

[40] H. Margenau, Phys. Rev. 48 (1935) 755.
[41] M.W. Klein, Phys. Rev. 173 (1968) 552.
[42] J.M. Ziman, Models of Disorder (Cambridge University Press, 1979).
[43] Goodness-of-Fit Techniques, eds. B.D. Agostino and M.A. Stephens (Dekker, New York, 1986).
[44] L.R. Walker and R.E. Walstedt, Phys. Rev. B 22 (1980) 3816.
[45] E.P. Wohlfarth and E.C. Stoner, Philos. Trans. R. Soc. (London) Ser. A 240 (1948) 599.
[46] R. Ferre, B. Barbara, D. Fruchart and P. Wolfers, J. Magn. Magn. Mater. 140–144 (1995) 385.